Journal of Casting & Materials Engineering Vol. 9 No. 3 (2025) 23–31
https://doi.org/10.7494/jcme.2025.9.3.23

Influence of Selected Corrosive Environment on the Scale Formation in Selected Materials Manufactured by Directed Energy Deposition 3D Printing Technology

Marcin Małysza [a, b *], **Ewa Rząd** [a], **Łukasz Zięba** [c]

[a] AGH University of Krakow, Faculty of Metals Engineering and Industrial Computer Science, 30 Mickiewicza Ave., 30-059 Krakow, Poland
[b] Lukasiewicz Research Network – Krakow Institute of Technology, 73 Zakopianska St., 30-418 Krakow, Poland
[c] Centrum B+R Grupy ARP S.A., 9 Tarnobrzeska St., 26-613 Radom, Poland
e-mail: marcin.malysza@kit.lukasiewicz.gov.pl

Received: 29 April 2025/Accepted: 28 July 2025/Published online: 19 September 2025.
This article is published with open access at AGH University of Science and Technology Journals.

Abstract

Additive technologies, and in particular Directed Energy Deposition (DED), are becoming an increasingly important tool for the rapid production of components operating in, among others, the energy, aviation, petrochemical industries, where components are exposed to extreme thermochemical conditions. In the article, the influence of various corrosive atmospheres atmospheric air, water vapor and SO_2-argon- mixture – on the process of scale formation on the surface of materials manufactured using Directed Energy Deposition (DED) technology is presented. The tests were carried out at a temperature of 600°C (for air and water vapor) and 300°C (for SO_2-argon atmosphere). The mass increase and surface damage was monitored. It has been shown that the chemical composition of materials, especially the content of alloying elements such as Cr and Ni, is crucial for corrosion resistance. The obtained results provide the basis for further optimization of the composition of powders used in additive manufacturing techniques, in terms of operating conditions in aggressive environments.

Keywords:

corrosion resistance, oxide scale, DED microstructure, sulfur atmosphere, high-temperature oxidation

1. INTRODUCTION

Recent years, have seen the dynamic development of additive manufacturing (AM) technologies, which have found wide application in materials engineering and heavy industry, including the energy sector [1–3]. One of the advanced 3D printing methods used to produce metal components is Directed Energy Deposition (DED). This method involves the simultaneous supply of material (in the form of metal powder or wire) and its local melting using a concentrated energy source, most often a laser, electron beam, or plasma. This process enables the precise fabrication of complex geometries and is widely used for the surfacing, regeneration, and modification of existing components. DED offers unique advantages over other AM techniques. Compared to Powder Bed Fusion (PBF), Directed Energy Deposition allows faster deposition rates and the capability to repair large parts, albeit with lower resolution. Binder Jetting, while effective for ceramics and composites, typically requires post-processing and lacks mechanical strength. In contrast, DED combines high deposition efficiency with structural integrity, making it suitable for applications in aerospace, power generation, and petrochemicals [4–6].

In the present study, a laser-based DED system was used, equipped with a 4 kW IPG fiber laser and a water-cooled coaxial deposition head, ensuring uniform material delivery and efficient heat management. The process was carried out on an RPMI machine featuring five-axis CNC control, an argon atmosphere glovebox with lower than 10 ppm of oxygen level, and dual-hopper powder feeders allowing continuous operation. The applied laser energy density was analyzed in a separate study and determined to be 1.717 J/mm^3 [7]. Other processing parameters, including a laser power of 1300 W, track width of 1.52 mm, and layer height of 0.5 mm, were selected according to the equipment manufacturer's recommendations. All of the analyzed materials were deposited in the form of powder.

The schematic presented in Figure 1 shows the metal powder is delivered directly into a melt pool created by a focused energy source a high-power laser. The material is deposited layer by layer onto the substrate, enabling the fabrication or repair of complex components with precise geometry [8]. The scale, as an oxide layer formed on the metal surface under the influence of certain conditions, plays an important role in the context of protecting the material from further corrosion. Its structure, chemical composition, adhesion and thickness determine the effectiveness of the protective barrier. At a temperature of 600°C, the stability of the scale, its resistance to loosening and the rate of its growth during operation are of

great importance [9–12]. Figure 2 shows a model of scale formation on the surface of the substrate [14].

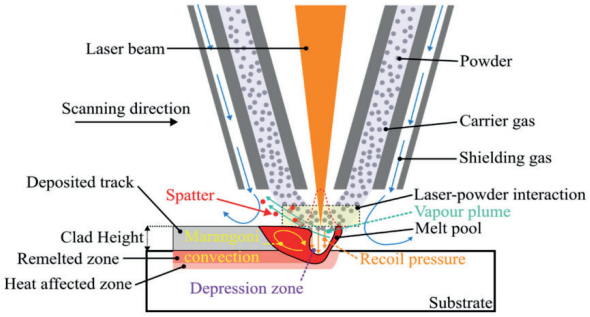

Fig. 1. Scheme of the AM process using the DED method [13]

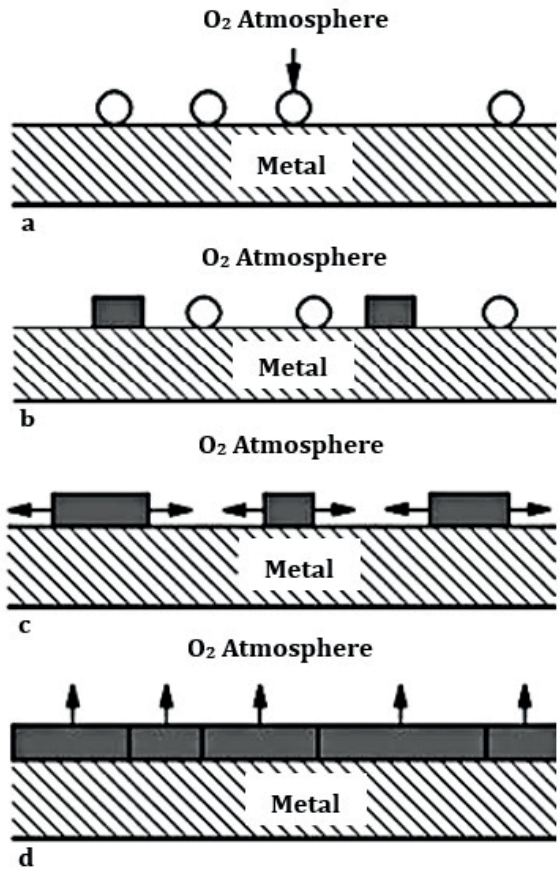

Fig. 2. Ideal model of the scale formation process [14]

Materials produced by the DED method are characterized by a specific microstructure resulting from the rapid melting and solidification of material layers. Characteristic features include a columnar texture, the presence of residual stresses, and local differences in chemical composition caused by the segregation of elements [15]. All factors affect the scale formation process and its subsequent changes under the specified operating conditions. The work uses measurements assessed in the context of scale formation, i.e. the rate of mass increase, and visual assessment of such factors as the presence of cracks or detached fragments of scale.

2. MATERIALS AND METHODS

Due to the increasingly widespread use of printed elements in very diverse working conditions, it was decided to conduct research in selected environmental conditions occurring in industrial applications. In order to assess the effect of the air atmosphere on the process of scale formation, laboratory tests were carried out under controlled exposure to high temperature (600°C) in the presence of atmospheric oxygen. The materials for the tests were prepared using DED additive technology, which made it possible to obtain samples with comparable geometric and structural parameters. Oxidation processes were carried out in a tube furnace, with a constant air flow, monitoring changes in the sample mass and analyzing the morphology and chemical composition of the resulting scale. The second modeled operating environment of the printed samples was the presence of water vapor, where 100% pure water vapor was passed through the furnace by pumping deionized water in a closed circuit. The third of the analyzed environments were the conditions induced by exposure in an atmosphere containing gaseous sulfur compounds (SO_2-argon). The samples were subjected to an aggressive environment at a temperature of 300°C and 600°C, which was intended to simulate conditions in power plants burning sulfur fuels. The oxidation and sulfurization processes were monitored by analyzing the mass increase. The tested samples were cleaned in isopropanol using an ultrasonic bath for 15 minutes at 40°C. After drying, the samples were carefully weighed using an analytical balance (accuracy 10^{-5} g). Materials produced by the DED method were selected for the tests, which, together with their chemical composition in the form of power and, are listed in Table 1. The samples were cut with a wet diamond disc and then sanded with sandpaper.

Table 1
Chemical compositions of selected materials obtained by the additive method

Name	Material	Cr	Ni	Cu	W	Mo	S	Co	Ti	Nb-Ta	Nb	Si	Mn	V	P	C	Bal.
1.x	CL92	15–17.5	3.5	3–5		0.1	–	–		0.15–0.45	–	0.1	0.1	–	–	0.05	Fe
2.x	X22CrMoV12-1	11.5	–	–		0.7	–	–	–	–	0.1	–	0.6	0.2	–	0.2	Fe
3.x	H13	5.0	–	–		–	–	0.1	–	–	–	–	0.3	0.35	–	0.4	Fe
4.x	18Ni300	–	18.3	–		4.8	–	8.9	0.8	–	–	–	–	–	–	0.003	Fe
5.x	Hastelloy X	21	14	–	0.5	9	–	1.0	0.15	–	–	–	0.1	–	–	0.07	Ni
6.x	316L	18	14	–	–	2.5	–	–	–	–	–	0.7	2.0	–	–	0.03	Fe
7.x	Bohler W360	–	0.1			3.0	0.4					0.3	0.3	0.6	0.02	0.5	Fe

2.1. Studies of the effect of steam on the scale formation process

The tests were carried out using the steam oxidation station shown in the diagram, Figure 3. During the experiment, 100% pure steam was generated by pumping deionized water from a tank placed under the furnace. Steam was passed through the furnace in a closed circuit at a rate of 2.833 ml/min. Deionized water with low electrical conductivity was used. The whole was sealed using stainless steel flanges equipped with a high-temperature gasket at both ends.

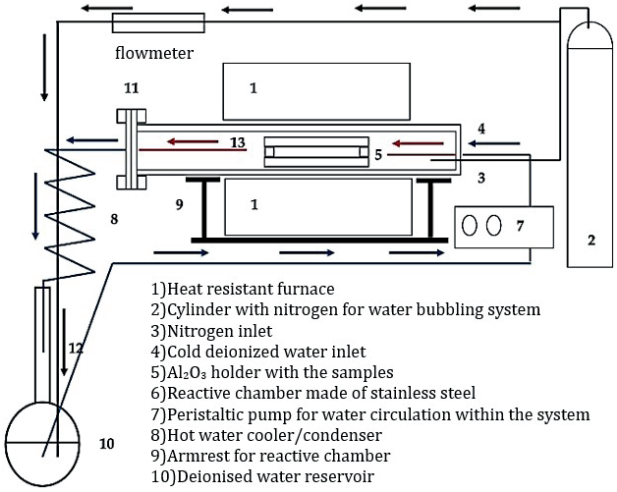

Fig. 3. Schematic diagram of the test stand for corrosion in a steam environment

Before the oxidation process in steam, the entire system was purged for at least 2 h with oxygen-free nitrogen (OFN) to remove moisture and atmospheric air remaining in the reaction chamber. During the tests, OFN purification was continued through a tank with deionized water to minimize the concentration of O_2-ions in the test system. Before the experiment, the furnace was calibrated to set the desired temperature and place the samples in the so-called "hot zone". The calibration process ensured that the samples were placed in the furnace at the test temperature with an accuracy of more or less 5°C. The tests were carried out at a temperature of 600°C for 500 h with breaks every 100 h (weight gain test). The samples were introduced into the hot zone of the furnace using a calibrated rod with a measured distance. After each interval, the samples were cooled freely to room temperature by turning off the power supply. The samples after oxidation were examined on a macro scale using: a macro lens and a Canon 70D digital single-lens camera equipped with a Canon MP-E 65 mm f/2.8 macro lens. Macro photos of each of the tested samples were taken after 100 h.

2.2. Studies on the effect of atmospheric air on the process of scale formation

Similarly to the previously conducted studies and apparatus, the samples were cleaned in isopropanol using an ultrasonic bath for 15 minutes at a temperature of 40°C. After drying, the samples were carefully weighed using an analytical balance (accuracy 10^{-5} g). Then, the experiment was carried out in the atmosphere of atmospheric air. Before the experiment, the furnace was calibrated to set the desired temperature and place the samples in the so-called "hot zone". The calibration process ensured that the samples were placed in the furnace at the test temperature with an accuracy of more or less 5°C. The tests were carried out at a temperature of 600°C for 500 h with breaks every 100 h (mass increase test). The samples were introduced into the hot zone of the furnace using a calibrated rod with a measured distance. After each interval, the samples were cooled to room temperature in a free manner by turning off the power supply. The samples after oxidation were examined on a macro scale using: a macro lens and a Canon 70D digital single-lens camera equipped with a Canon MP-E 65 mm f/2.8 macro lens.

2.3. Studies on the effect of the atmosphere of sulfur compounds on the process of scale formation

A study of high-temperature corrosion was carried out in a flowing gas mixture containing SO_2-argon. The SO_2 content in the gas mixture was 0.25% by volume, at a flow rate of 50 ml/min and a heating rate of 5°C/min. The diagram of the experimental stand for high-temperature sulphation studies is shown in Figure 4.

The test rig consists of an electric tube furnace (CARBOLITETM) with wire heating elements, a reactive gas tank, a gas supply pipe equipped with a flow control system, and a cooling unit. The reactive gas tank (99.75% synthetic air – 0.25% SO_2) was obtained from the gas supplier (Air Products). The gas flow through the furnace was controlled by a rotameter installed between the gas cylinder and the furnace. The flow rate was set at 50 Nml/min (Nml/min at 293.15 K, 1 bar – standard conditions). The test specimens were placed on a refractory alumina (99.5% Al_2O_3) holder. The temperature in the hot zone of the furnace was monitored by a programmable EUROTHERM controller. The furnace was carefully calibrated before the tests. For safety reasons, the reaction chamber (alumina tube) of the furnace was enclosed in a 316-L stainless steel vessel, closed at both ends with 316-L stainless steel flanges, locked with four screws. The exiting gas mixture was passed through a NaOH solution to neutralize and flush out SO_2, and then directed to the ventilation system. The samples were tested in an SO_2-argon atmosphere for 200 h. The tests consisted of four cycles of 50 h/cycle. The samples were placed in the furnace at room temperature and suitably heated to 300°C, with a ramp of 5°C/min, and held at the appropriate temperature for 50 h; then the samples were removed from the furnace and imaged. Before testing, the samples were accurately measured with an electronic micrometer, then the samples were cleaned in an ultrasonic bath for 15 min at 40°C and weighed using a high-precision Sartorius CPA225D electronic balance. Post-exposure imaging was performed using a Canon EOS 70D single-lens reflex camera coupled with a Canon MP-E 65 mm f/2.8 macro lens.

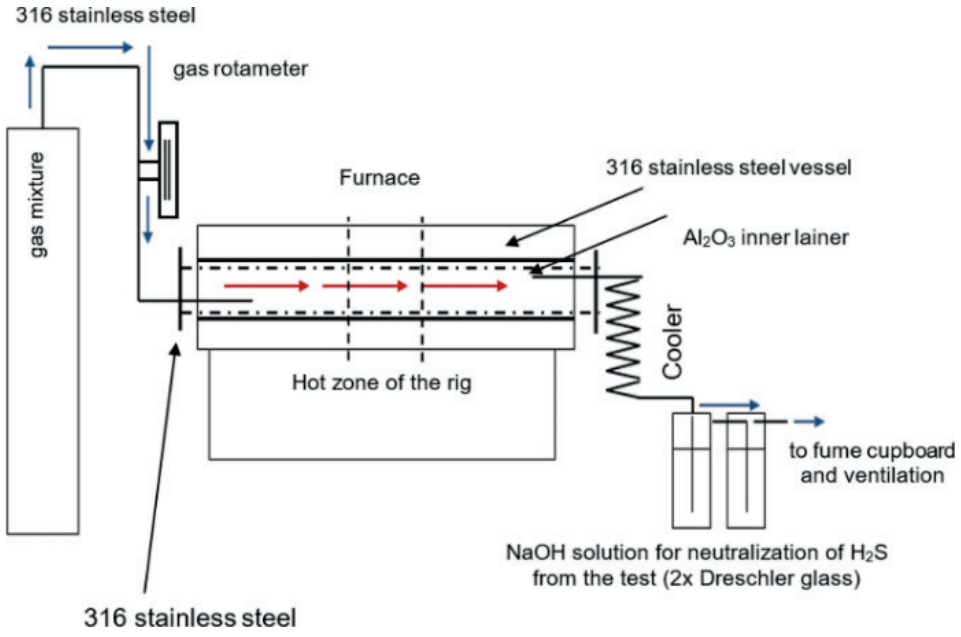

Fig. 4. Schematic of the SO_2-argon-corrosion test rig

3. RESULTS AND DISCUSSION

Corrosion processes occurring in atmospheres containing sulfur compounds are particularly aggressive towards metallic materials. Corrosion products – sulfides and oxides – can form protective scale, but its effectiveness depends largely on the chemical composition of the material. In this context, alloying elements such as chromium (Cr) and nickel (Ni) play an important role. Analysis of the results showed clear differences in the behavior of the scale depending on the environment. In a clean air atmosphere, samples with a high Cr content (e.g. 316L and Hastelloy X) showed minimal mass gains, which indicates the effective formation of a Cr_2O_3 layer, characterized by good adhesion and stability at high temperature. For samples with a lower Cr content (e.g. H13), larger mass gains and delamination of the scale were observed, which may be the effect of the porous structure of Fe oxides and unstable mixed scales. In a water vapor environment, the effect of H_2O presence was more destructive – especially for samples with a low Ni content. Steam accelerates the oxidation process by facilitating ion transport through the scale, and can also lead to the formation of Fe-rich oxides, which are less protective and more susceptible to cracking. Scale spalling and cracking were visible for samples 2.4–4.4, indicating a lack of continuity of the protective layer. Samples containing significant amounts of Ni (e.g. 18Ni300 and Hastelloy X) showed good resistance – the presence of Ni promotes homogenization of the scale and limits its delamination. The greatest differences were observed under conditions of exposure to an atmosphere of sulfur compounds (SO_2). The formation of sulfides leads to more aggressive degradation, and the corrosion layers are less stable and more expansive. Samples 3.1 and 4.1 showed mass gain and intensive corrosion, confirming the high reactivity of the material in this environment. Materials with high Cr and Ni contents (1.1 and 6.1) again showed the greatest resistance – the protective layers formed faster and were less susceptible to mechanical damage. A significant factor influencing the results was the DED microstructure – the presence of internal stresses and element segregation zones could locally affect the development of the scale. Further microstructural studies (e.g. SEM/EDS, XRD) are planned to fully understand the mechanisms of local degradation of the printed material.

Due to the development of 3D printing technology, interest in their durability in different operating conditions is growing, particularly in terms of corrosion resistance. The wide range of materials that can be used in additive technologies requires various types of testing. Materials such as 316L stainless steel, AlSi10Mg aluminum alloys, and M300 tool steel, manufactured by laser powder sintering, are used in the marine, aerospace, and medical industries. However, a key issue is their susceptibility to various forms of corrosion. To expand on the topic presented in this paper, a brief description of various studies related to material corrosion is provided below. Research conducted by Lawrence Livermore National Laboratory has shown that 3D printed 316L steel is susceptible to pitting resulting from the presence of slag remaining during the powder remelting process. These surface defects promote the initiation of local damage, which can be exacerbated in a marine environment. Importantly, slag removal processes typical of conventional manufacturing methods (e.g., grinding) are not readily applicable to 3D printed parts [16]. Other studies, focusing on the effect of TiAlV alloy surface treatment, indicate that treatments such as anodizing can significantly increase the corrosion resistance of components, even after prior chemical etching. Anodized surfaces demonstrated stable passive behavior and no development of active corrosion spots [17]. Corrosion-fatigue tests of the AlSi10Mg alloy yielded equally interesting results. It was observed that mechanically treated samples (removal of layers rich in porosity and unmelted powder) exhibited significantly higher fatigue resistance and lower susceptibility to crack initiation at corrosion pits.

Untreated samples were significantly more susceptible to mechanical damage due to corrosion, especially in sequential and combined tests [18]. Studies on M300 steel, in turn, indicated that both the laser power used during printing and the surface treatment significantly influenced the rate and nature of corrosion. Generally, increasing laser power led to a decrease in corrosion resistance, and unpolished samples exhibited greater mass loss in long-term tests [19]. It is discernible that the temperature of the corrosive environment also played a significant role – higher temperatures accelerated the processes, as shown in the study summary below.

3.1. Results of the effect of steam on the scale formation process

The summary of the photos taken is presented in Table 2. After oxidation, the materials were covered with oxide scale. For materials 2.4–4.4, chips and cracks were observed on the surface of the annealed materials. The remaining samples were characterized by continuous, compact scale. The changes in the mass of the tested samples as a result of oxidation in a water vapor atmosphere at a temperature of 600°C for 100–500 h are presented in Figure 5.

Table 2
Macro photos for the tested materials oxidized at T = 600°C in a water vapor atmosphere and the mass change

Water vapor, T = 600°C						
No.	0 h	100 h	200 h	300 h	400 h	500 h
1.4	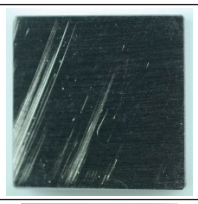	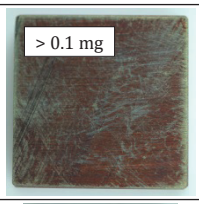 > 0.1 mg	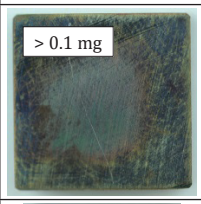 > 0.1 mg	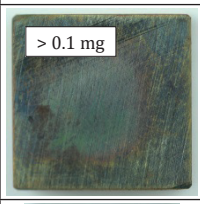 > 0.1 mg	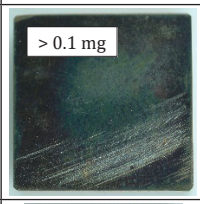 > 0.1 mg	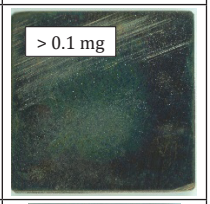 > 0.1 mg
2.4	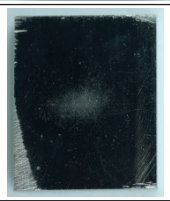	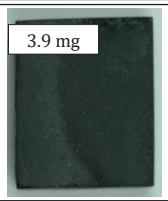 3.9 mg	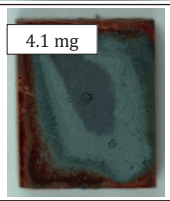 4.1 mg	 4.5 mg	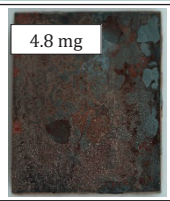 4.8 mg	 5 mg
3.4	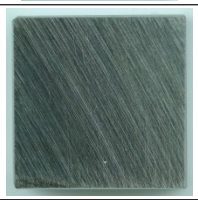	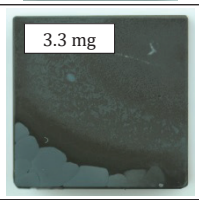 3.3 mg	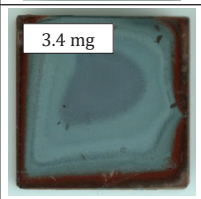 3.4 mg	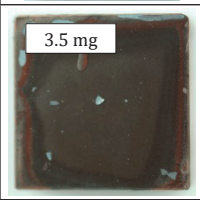 3.5 mg	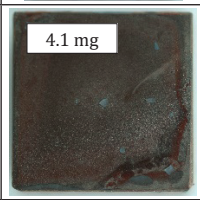 4.1 mg	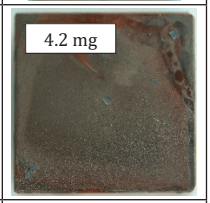 4.2 mg
4.4	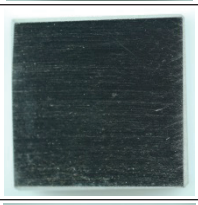	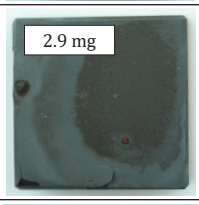 2.9 mg	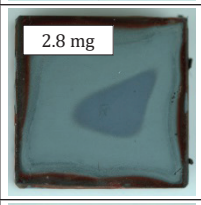 2.8 mg	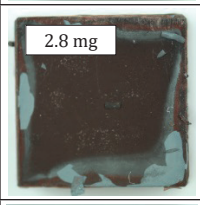 2.8 mg	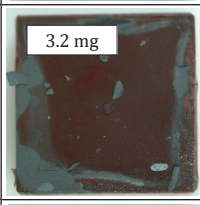 3.2 mg	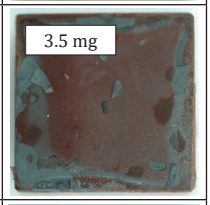 3.5 mg
5.4	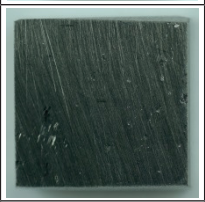	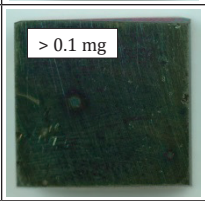 > 0.1 mg	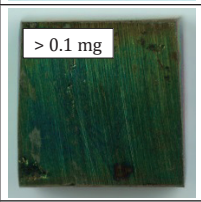 > 0.1 mg	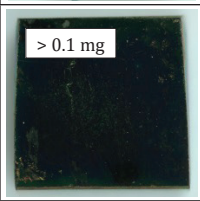 > 0.1 mg	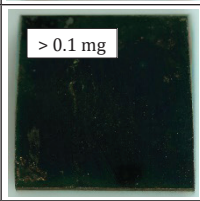 > 0.1 mg	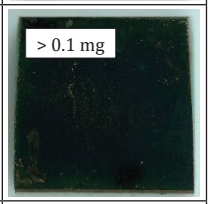 > 0.1 mg
6.4		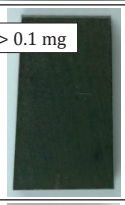 > 0.1 mg	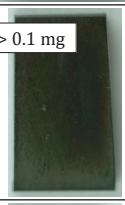 > 0.1 mg	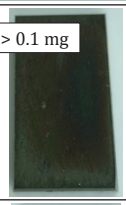 > 0.1 mg	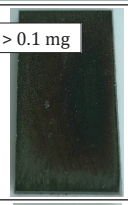 > 0.1 mg	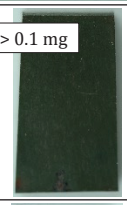 > 0.1 mg
7.4		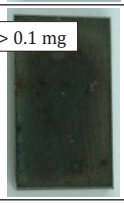 > 0.1 mg	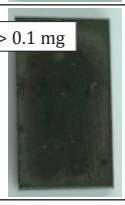 > 0.1 mg	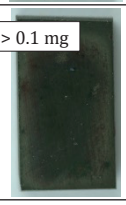 > 0.1 mg	> 0.1 mg	> 0.1 mg

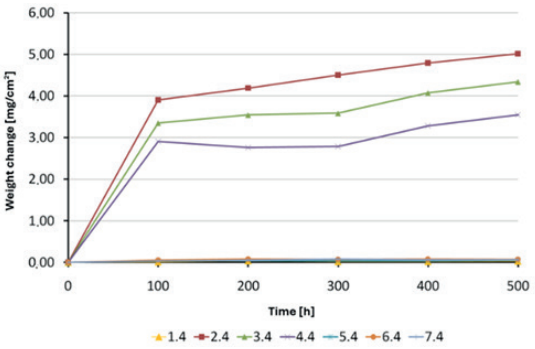

Fig. 5. Observed changes in the mass of samples subjected to oxidation in a water vapor atmosphere at a temperature of 600°C for 100–500 h

The course of the oxidation process of the tested materials at a temperature of 600°C in a water vapor atmosphere. For samples 1.4 and 5.4–7.4, negligible mass increases were recorded. The surfaces of the samples were continuous, without chips. The analyzed materials were characterized by the highest corrosion resistance. For samples 2.4–4.4, mass increases of 3 mg/cm^2 to 5 mg/cm^2 were observed. During the experiment, delamination of the produced scale was observed.

3.2. Results on the effect of atmospheric air on the process of scale formation

Table 3 summarizes the macro images for the tested samples.

Table 3
Macro images for the tested materials oxidized at T = 600°C in the atmosphere of atmospheric air and the mass change

Atmospheric air, T = 600°C						
No.	0 h	100 h	200 h	300 h	400 h	500 h
1.2		> 0.1 mg	> 0.1 mg	> 0.1 mg	> 0.1 mg	> 0.1 mg
2.2		> 0.1 mg	> 0.1 mg	> 0.1 mg	> 0.1 mg	> 0.1 mg
3.2		> 0.1 mg	> 0.1 mg	> 0.1 mg	> 0.1 mg	> 0.1 mg
4.2		2.3 mg	1.0 mg	1.5 mg	1.9 mg	1.0 mg
5.2		> 0.1 mg	> 0.1 mg	> 0.1 mg	> 0.1 mg	> 0.1 mg
6.2		> 0.1 mg	> 0.1 mg	> 0.1 mg	> 0.1 mg	> 0.1 mg
7.2		0.5 mg	0.5 mg	3.0 mg	4.9 mg	5.9 mg

The changes in the mass of the tested samples as a result of oxidation in an air atmosphere at a temperature of 600°C for 100–500 h are presented in Figure 6.

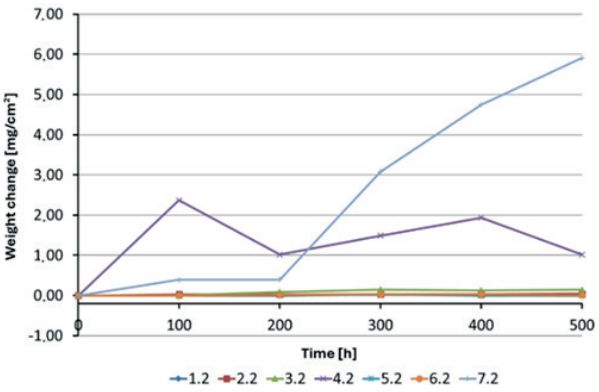

Fig. 6. Observed changes in the mass of samples subjected to oxidation in an air atmosphere at a temperature of 600°C for 100–500 h

The course of the oxidation process of the tested materials at a temperature of 600°C in an air atmosphere allows us to note that for samples 1.2; 2.2; 3.2 and 5.2 and 6.2, negligible mass increases were recorded. The surfaces of the samples were continuous, without splinters. The analyzed materials were characterized by the highest corrosion resistance. For samples 4.2 and 7.2, mass increases of the order of 2 6 mg/cm^2 and 6 mg/cm^2 were observed. During the experiment, delamination of the produced scale was observed.

3.3. Results on the effect of the atmosphere of sulfur compounds on the process of scale formation

Table 4 summarizes the macro images for the tested samples. The dependence of the mass change of the tested samples as a result of high-temperature corrosion in an 0.25%SO_2-argon atmosphere at temperatures of 100–300°C for 50–200 h was also plotted and presented in Figure 7.

Table 4
Macro images for the tested materials at T = 300°C in a 0.25%- SO_2-argon atmosphere and the mass change

0.25% SO_2-argon, T = 300°C					
No.	0 h	50 h	100 h	150 h	200 h
1.1	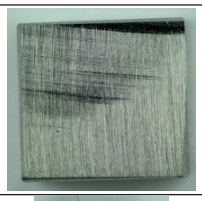	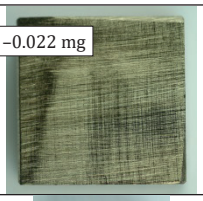 –0.022 mg	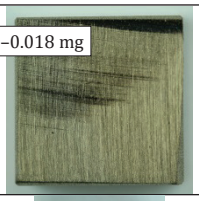 –0.018 mg	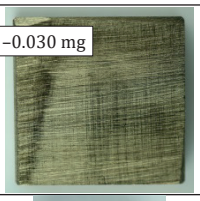 –0.030 mg	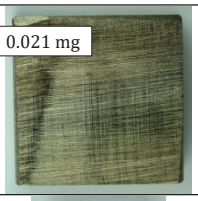 0.021 mg
2.1		 –0.018 mg	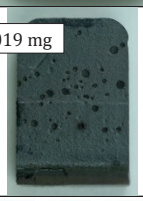 0.019 mg	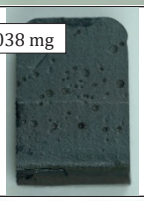 0.038 mg	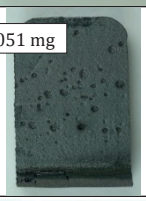 0.051 mg
3.1		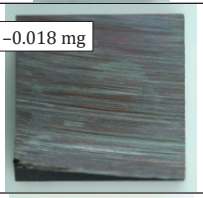 –0.018 mg	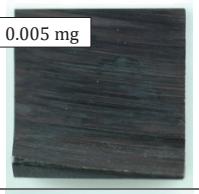 0.005 mg	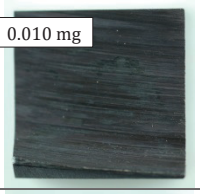 0.010 mg	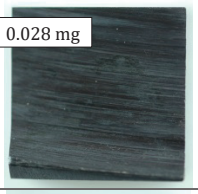 0.028 mg
4.1	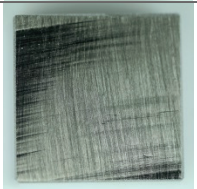	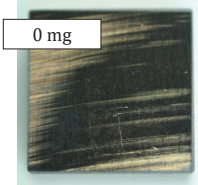 0 mg	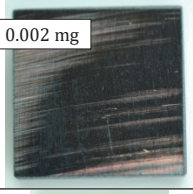 0.002 mg	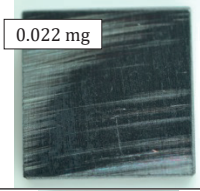 0.022 mg	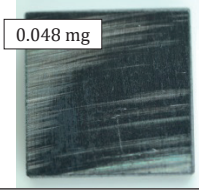 0.048 mg
5.1		 –0.022 mg	 –0.024 mg	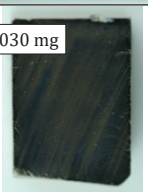 –0.030 mg	 –0.021 mg
6.1	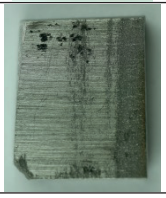	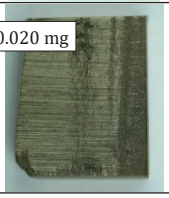 –0.020 mg	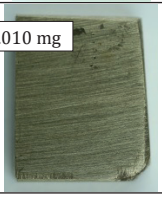 0.010 mg	 0.008 mg	 0.028 mg

Table 4 (cont.)

0.25% SO_2-argon, T = 300°C					
No.	0 h	50 h	100 h	150 h	200 h
7.1		 0.050 mg	 0.072 mg	 0.030 mg	 0.082 mg

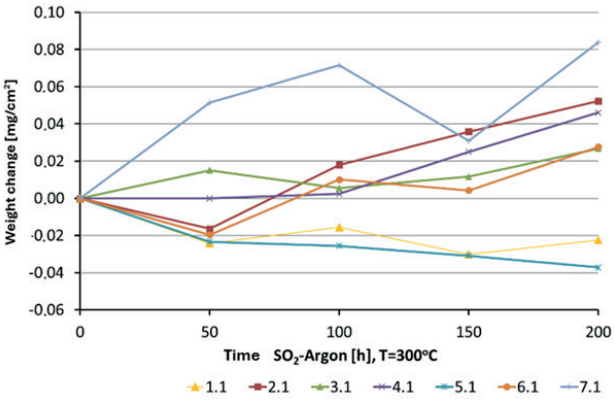

Fig. 7. High-temperature corrosion process of the tested materials at 300°C in a 0.25% SO_2-argon atmosphere

The courses of the individual curves reveal significant differences in susceptibility to corrosion. Samples 2.1; 3.1; 4.1; 7.1 show a very similar nature of mass increase, which suggests that the material has moderate resistance to oxidation in the presence of sulfur. Sample 7.1 shows a more rapid mass increase over time, which indicates intensive scale formation and lower resistance to corrosive gases. In turn, samples 1.1 and 6.1 show a smaller mass increase – especially in the later h of the experiment – which may be evidence of more effective formation of a passive layer limiting further corrosion.

4. CONCLUSIONS

This study shows the corrosion resistance of DED-manufactured alloys in different oxidizing and sulfur-containing environments. The results highlight the correlations between alloy composition and the mechanisms governing oxidation behavior:

- The corrosion resistance of DED-manufactured alloys significantly depends on the chemical composition, particularly the content of chromium (Cr) and nickel (Ni), and the nature of the corrosive environment.
- Alloys such as Hastelloy X and 316L (high in Cr and Ni) demonstrated minimal mass gain lower than 1.5 mg/cm^2) and superior scale integrity under all tested conditions, including the SO_2-rich environment, due to the formation of stable Cr_2O_3 and NiO layers.
- In contrast, alloys with low Cr/Ni content (e.g., H13, Bohler W360) showed substantial mass increase (up to 6 mg/cm^2) and visible scale cracking, especially in water vapor and sulfur-containing atmospheres, indicating limited oxidation resistance.
- The most aggressive environment was the argon-SO_2 mixture, where sulfide formation led to rapid scale growth and spallation. Only Ni-rich materials maintained structural integrity under such exposure.
- The unique microstructural features resulting from DED – including residual stresses and chemical inhomogeneities – may promote localized corrosion and warrant further investigation using advanced microscopy and spectroscopy (e.g., SEM/EDS, XRD).
- These findings contribute to the development of corrosion-resistant alloys tailored for additive manufacturing. The results serve as a foundation for selecting or designing powder compositions optimized for harsh industrial applications, including turbine blades, petrochemical tubing, and boiler components.
- Future work should include in-situ oxidation monitoring, long-term mechanical testing of oxidized layers, and correlation with thermal fatigue performance under cyclic loading conditions.

ACKNOWLEDGEMENTS

The presented results were developed as part of the project financed by the National Centre for Research and Development, MAZOWSZE/0157/19-00 entitled "Development and implementation of a complete technological line for incremental recovery, regeneration and improvement of parts of manufacturing installations for companies in the petroleum and chemical industries – in order to reduce the time and costs of their acquisition".

REFERENCES

[1] Singh Om P., Ahmed Sheikh M. & Abhilash M. (2015). Modern 3D printing technologies: Future trends and developments. *Recent Patents on Engineering*, 9(2), 91–103. DOI: https://doi.org/10.2174/1872212109666150213000747.

[2] Wanlu C. & Y. Zhang (2019.) Development and application of 3D printing technology in various fields. *Journal of Physics: Conference Series*, 1303, 012032. DOI: https://doi.org/10.1088/1742-6596/1303/1/012032.

[3] Woźniak J., Budzik G., Przeszłowski Ł. & Chudy-Laskowska K. (2021). Directions of the development of the 3D printing industry as exemplified by the Polish market. *Management and Production Engineering Review*, 12(2), 98–106. DOI: https://doi.org/10.24425/mper.2021.137682.

[4] Freire B., Babcinschi M., Ferreira L., Senaris B., Vidal F. & Neto P. (2020). Direct energy deposition: A complete workflow for the additive manufacturing of complex shape parts. *Procedia Manufacturing*, 51, 671–677. DOI: https://doi.org/10.1016/j.promfg.2020.10.094.

[5] Svetlizky D., Das M., Zheng B., Vyatskikh A.L., Bose S., Bandyopadhyay A., Schoenung J.M., Lavernia E.J., & Eliaz N. (2021). Directed energy deposition (DED) additive manufacturing: Physical characteristics, defects, challenges and applications. *Materials Today*, 49(11), 271–295., DOI: https://doi.org/10.1016/j.mattod.2021.03.020.

[6] Novotný V., Bryksí Stunová B., Schastlivtseva E. & Zikmund P. (2018). 3D printed parts for power industry. Technological forum 2018, Dubovice, Czech Republic. URL: https://www.researchgate.net/publication/327282182_3D_Printed_Parts_for_Power_Industry

[7] Małysza M., Żuczek R., Wilk-Kołodziejczyk D., Jaśkowiec K., Bitka A., Głowacki M., Zięba Ł. & Pysz S. (2024). Application of a 3D-printed part with conformal cooling in high-pressure die casting mould and evaluation of stress state during exploitation. *Materials*, 17(23), 5988. DOI: https://doi.org/10.3390/ma17235988.

[8] Mu'az Imran M., Che Idris A., Chandratilak De Silva L., Kim Y.-B. & Emeroylariffion Abas P. (2024). Advancements in 3D printing: Directed energy deposition techniques, defect analysis, and quality monitoring. *Technologies*, 12(6), 86. DOI: https://doi.org/10.3390/technologies12060086.

[9] Dudziak T., Hussain T., Simms N.J., Syed A.U. & Oakey J.E. (2014). Fireside corrosion degradation of ferritic alloys at 600°C in oxy-fired conditions. *Corrosion Science*, 79, 184–191. DOI: https://doi.org/10.1016/j.corsci.2013.11.005.

[10] Dudziak T.P. (2016). Steam oxidation of Fe-based materials. In: Ahmad Z. (Ed.), *High Temperature Corrosion*. In: Ahmad Z., *High Temperature Corrosion*, IntechOpen. DOI: https://doi.org/10.5772/62935.

[11] Kane K., Stack P., Schappel D., Montoya K., Mouche P., Sooby E. & Tarrani K. (2021). Oxidation of 3D-printed SiC in air and steam environments. *Journal of the American Ceramic Society*, 104(5), 2225–2237. DOI: https://doi.org/10.1111/jace.17632.

[12] Shi H., Jianu A., Weisenburger A., Tang C., Heinzel A., Fetzer R., Lang F., Stieglitz R. & Müeller G. (2019). Corrosion resistance and microstructural stability of austenitic Fe–Cr–Al–Ni model alloys exposed to oxygen-containing molten lead. *Journal of Nuclear Materials*, 524, 177–190. DOI: https://doi.org/10.1016/j.jnucmat.2019.06.043.

[13] Reddy Madara S. & Pon Selvan C. (2017). Review of recent developments in 3-D printing of turbine blades. *European Journal of Advances in Engineering and Technology*, 4(7), 497–509. URL: https://www.researchgate.net/publication/318960215.

[14] Dai J., Zhu J., Chen C. & Weng F. (2016). High temperature oxidation behavior and research status of modifications on improving high temperature oxidation resistance of titanium alloys and titanium aluminides: A review. *Journal of Alloys and Compounds*, 685, 784–798. DOI: https://doi.org/10.1016/j.jallcom.2016.06.212.

[15] Saboori A., Aversa A., Marchese G., Biamino S., Lombardi M. & Fino P. (2020). Microstructure and mechanical properties of AISI 316L produced by directed energy deposition-based additive manufacturing: A Review. *Applied Science,* 10(9), 3310. DOI: https://doi.org/10.3390/app10093310.

[16] Sen-Britain S., Cho S., Kang S., Qi Z., Khairallah S., Rosas D., Som V., Li T.T., Qiu S.R., Wang Y.M., Wood B.C. & Voisin T. (2024). Critical role of slags in pitting corrosion of additively manufactured stainless steel in simulated seawater. *Nature Communications*, 15, 867. DOI: https://doi.org/10.1038/s41467-024-45120-6.

[17] Fojt J., Hybasek V., Kacenka Z. & Pruchova E. (2020). Influence of surface finishing on corrosion behaviour of 3D printed TiAlV alloy. *Metals*, 10(11), 1547. DOI: https://doi.org/10.3390/met10111547.

[18] Linder C., Vucko F., Ma T., Proper S. & Dartfeldt E. (2023). Corrosion-fatigue performance of 3D-printed (L-PBF) AlSi10Mg. *Materials*, 16(17), 5964. DOI: https://doi.org/10.3390/ma16175964.

[19] Żaba K., Szymański K., Balcerzak M., Różycka I., Kuczek Ł. & Żabiński P. (2024). Effect of surface finishing on the corrosion resistivity of 3D printed M300 steel. *Materials*, 17(24), 6047. DOI: https://doi.org/10.3390/ma17246047.